

Electronic structures of antiperovskite superconductors: MgXNi_3 ($\text{X}=\text{B}, \text{C}, \text{N}$)

J. H. Shim and B. I. Min

Department of Physics, Pohang University of Science and Technology, Pohang 790-784, Korea

We have investigated electronic structures of a newly discovered antiperovskite superconductor MgCNi_3 and related compounds MgBNi_3 and MgNNi_3 . In MgCNi_3 , a peak of very narrow and high density of states is located just below E_F , which corresponds to the π^* antibonding state of Ni-3d and C-2p but with the predominant Ni-3d character. The prominent nesting feature is observed in the Γ -centered electron Fermi surface of an octahedron-cage-like shape that originates from the 19th band. The estimated superconducting parameters based on the simple rigid-ion approximation are in reasonable agreement with experiment, suggesting that the superconductivity in MgCNi_3 is described well by the conventional phonon mechanism.

71.25.Pi, 74.25.Jb, 74.70.Ad

Recently, He *et al.*¹ have discovered a new intermetallic superconductor MgCNi_3 with the transition temperature T_C of 8K, which has the antiperovskite structure. Because it has a large proportion of Ni per unit cell, it is expected that the magnetic fluctuation would be important in determining the superconducting behavior. This system is reminiscent of another Ni-based superconductors $\text{LnNi}_2\text{B}_2\text{C}$ ($\text{Ln} = \text{Y}, \text{Tm}, \text{Er}, \text{Ho}, \text{Lu}$)²⁻⁴. The band calculations indicate that very large and narrow energy peak in the density of states (DOS) is located just below the Fermi energy E_F which has mainly the Ni 3d character^{5,6}. The behavior of the upper critical field $H_{c2}(T)$ can be well fitted with the conventional BCS expression⁷, whereas the zero-bias conductance peak observed below T_C suggests that MgCNi_3 is likely to be a non-s wave superconductor⁸.

With Cu doping (electron doping) on Ni-site, T_C decreases systematically, but with Co doping (hole doping), the superconductivity disappears abruptly for doping of only 1%⁵. In the case of Co doping, there is no evidence that the quenching of superconductivity is related to magnetism. Furthermore, it is observed that the superconductivity of MgC_xNi_3 is sensitive to the content of C; it disappears between $x=0.96$ and $x=0.90$ ¹.

To understand the mechanism of the superconductivity in MgCNi_3 , we have investigated systematically the electronic structures of MgXNi_3 ($\text{X}=\text{B}, \text{C}$ and N), which have different number of valence electrons, but have the similar band structures. Using the linearized muffin-tin orbital (LMTO) band method in the local density approximation (LDA), we have obtained band structures, DOSs, and Fermi surfaces, and discussed the bonding characters. Muffin-tin orbitals up to d -states for Mg, C, and up to f -states for Ni are included in the LMTO band calculations. We have also estimated superconducting

parameters based on the rigid-ion approximation. We have considered cubic MgCNi_3 with the lattice constant of 3.81\AA ¹ and employed the atomic radii of 3.20, 1.54 and 2.49\AA for Mg, C and Ni, respectively. The same structural parameters are used for all MgXNi_3 .

MgCNi_3 has the cubic antiperovskite structure: Mg at (0 0 0), C (0.5 0.5 0.5), and Ni at (0.5 0.5 0), (0.5 0 0.5) and (0 0.5 0.5). It is called as an antiperovskite structure because the transition metals are located at the corners of the octahedron cage in contrast to the ordinary perovskite structure⁹. Without C located at the center of cubic cell, MgNi_3 is a simple ordered intermetallic compound with fcc structure (Cu_3Au -type). Without C, the Ni-3d band of MgNi_3 is very narrow, leading to a magnetic ground state with Ni magnetic moment of $0.43\mu_B$ ¹⁰. By inserting C, two carbons become nearest neighbors of Ni, and thus it is expected that Ni-3d and C-2p electrons are strongly hybridized.

Total and projected local DOS of MgCNi_3 are provided in Fig. 1. The overall shape of the total DOS is similar to those of Hayward *et al.*⁵ and Dugdale and Jarlborg⁶. The peaks near -7eV and 4eV correspond to σ bonding and antibonding states, respectively, of Ni-3d and C-2p states. On the other hand, the peaks near -4eV correspond to π bonding states of Ni-3d and C-2p. The π^* antibonding states are located just below E_F , yielding the high DOS at E_F ($N(E_F)$) of 5.34 [states/eV]. The contribution of Ni-3d states to the DOS at E_F is as much as 76%. Small amount of C-2p states are hybridized with Ni-3d states. Because the peak just below E_F is very high and narrow, this system is expected to be unstable by small perturbation. The peak is located $\sim 60\text{meV}$ below E_F , and about 0.5 electrons are occupied between the peak and E_F . The stoner parameter S , defined as $S \equiv N(E_F)I_{XC}$ with I_{XC} denoting the intra-atomic exchange-correlation integral, is 0.64. Indeed the filling of holes in a rigid band scheme produces the magnetic instability. That is, replacing Ni by a virtual atom with atomic number 27.93 (corresponding to Co 7% doping) yields the stoner parameter larger than 1.00¹⁰.

The band structure of MgCNi_3 along the symmetry line of the simple cubic Brillouin zone is shown in Fig. 2. The band near -12eV corresponds to C-2s states, while the dispersive bands in the range of -7eV to -4eV are due to C-2p states. Only two bands (the 18th and 19th bands), which have mainly Ni-3d character, cut the Fermi level. These two bands are confined between -0.5eV and 1.0eV , and available states in these bands are about four. Hence, in the rigid band scheme, small electron or hole doping will produce the carriers with the 18th and the 19th band character. The 18th band is relatively flatter

than the 19th band, and so the Ni-3*d* character is stronger in the 18th band.

Figure 3 presents the Fermi surfaces of the 18th (a) and the 19th bands (b) in the simple cubic Brillouin zone. The 18th band gives rise to a clover-like hole surface centered at X of each cubic face and small hole pockets along the (111) directions. With increasing the Fermi level (electron doping), the areas of these hole Fermi surfaces decrease, reducing $N(E_F)$. In opposite, with decreasing the Fermi level (hole doping), the Fermi surface areas increase, enhancing $N(E_F)$. When decreasing the Fermi level further below the DOS peak, the crossing of each hole surface occurs, converting it to electron surface and decreasing Fermi surface. On the other hand, the 19th band yields an octahedron-cage-like electron surface centered at Γ and additional narrow electron surfaces along the Brillouin zone edges (Fig. 3(b)). As compared to the case of the 18th band, the 19th band shows a rather small change in the Fermi surface topology with varying the Fermi level position due to its more dispersive band character. The Fermi surface topology obtained in the present study is qualitatively similar to those of Dugdale and Jarlborg⁶.

The most notable in Fig. 3(b) is the prominent nesting feature along the (110) direction observed in the *ab* plane of the Γ -centered Fermi surface with the octahedron-cage-like shape. In fact, this is contrary to the report by Dugdale and Jarlborg⁶ who have not observed the obvious nesting feature in the Fermi surface of the 19th band. As mentioned above, the detailed shapes of the Fermi surfaces are very sensitive to the position of the Fermi level, because of the very sharp DOS peak near E_F . Presumably the difference between two results arises from the different band parameters employed in the LMTO band calculations, such as atomic radii, number of k-points, energy parameters, and so on. In any case, the present result reveals that the system is in the vicinity of the Fermi surface nesting, if not complete in undoped MgCNi₃. It is well known that the system with the Fermi surface nesting can be strongly correlated with various instabilities: the structural transition (the charge density wave instability) or the spin density wave instability. It is thus expected that MgCNi₃ may be susceptible to one of the above instabilities. However, until now, any evidence of magnetic or structure transition has not been reported^{5,11}. This aspect remains to be resolved.

We have seen that the DOS peak near E_F is produced by the hybridization of Ni-3*d* and C-2*p* states. In MgCNi₃, the bands from -0.5eV to 1.0eV are almost half-filled: two electron states out of four available states are occupied. To explore the doping effect with varying the number of valence electrons, we have investigated electronic structures of MgXNi₃ (X = B, C, N). Figure 4 provides the DOSs for MgXNi₃. It is seen that the effect of changing X is mainly a variance of the Fermi level with respect to the DOS peak. The shape of DOS is perturbed a little, which indicates that the rigid band scheme would work well in this system.

The B-2*p* state in MgBNi₃ is located higher in energy than the C-2*p* state of MgCNi₃, and so the hybridization with Ni-3*d* is stronger. Hence the band is more dispersive and accordingly the DOS peak becomes smeared. Although the Fermi level in MgBNi₃ is located very close to the DOS peak, the DOS at E_F , 4.79 [states/eV], is comparable to that of MgCNi₃ (5.34 [states/eV]) (Table I). Hence the magnetic instability does not occur either in MgBNi₃. As described before, the effective hole doping in MgBNi₃ converts a hole Fermi surface of the 18th band to an electron Fermi surface, and an electron surface of the 19th band is reduced smaller. In MgNNi₃, the N-2*p* state is located a bit lower in energy than the C-2*p* state of MgCNi₃, yielding reduced bandwidths of both the 18th and the 19th band. By the effective electron doping in MgNNi₃, the DOS at E_F is reduced to 3.63 [states/eV] (Table I). The contribution of the 18th band to the DOS at E_F is almost negligible and the Fermi surface of the 19th band, which gives the main contribution to the DOS at E_F , is changed to a hole surface.

We have explored superconducting properties of MgXNi₃ based on the rigid-ion approximation¹². We have estimated the superconducting parameter $\eta_\alpha = N(E_F)\langle I_\alpha^2 \rangle$, where $\langle I_\alpha^2 \rangle$ is the average electron-ion interaction matrix element for the α -th ion. Table II provides the calculated η_α for each MgXNi₃. It is seen that the contribution of Ni-3*d* states to the superconductivity is most important and η_{Ni} is the largest for MgCNi₃. This is consistent with the observed trend that both the electron and hole dopings on MgCNi₃ suppress the superconductivity. By increasing the atomic number from B, C to N, the contribution of X-2*p* states increases, while that of Ni-3*d* increases first and then decreases. Due to light ionic masses of X, even the small increase in η_X affects the superconducting property substantially. Therefore, effectively electron doped system MgNNi₃, once synthesized successfully in the antiperovskite structure, would have comparable T_C to MgCNi₃.

One can evaluate the electron-phonon coupling constant λ_{ph} by using the McMillan's formula $\lambda_{ph} = \sum_\alpha \eta_\alpha / M_\alpha \langle \omega_\alpha^2 \rangle$, where M_α is an ionic mass and $\langle \omega_\alpha^2 \rangle$ is the relevant phonon frequency¹³. Since there has been no information on the relevant phonons, we instead use the average phonon frequency $\langle \omega^2 \rangle \simeq \Theta_D^2/2$, where Θ_D is the Debye temperature. However, even the value of Θ_D is not available. Albeit very crude, one can estimate Θ_D from the specific heat data¹: ~ 300 K from the graph of C/T vs. T^2 . Using these informations for MgCNi₃, one obtains $\lambda_{ph} = 1.56$, and then the McMillan's T_C formula with an effective electron-electron interaction parameter $\mu^* = 0.13$ gives rise to $T_C = 23$ K. These values seem to be too large, as compared to experimental T_C and the estimated $\lambda_{ph} \sim 0.8$ from the specific heat data¹. Note, however, that λ_{ph} strongly depends on the choice of the Debye temperature. As shown in Table II, with a choice of larger $\Theta_D = 400$ K, one obtains $\lambda_{ph} = 0.77$ and $T_C = 11$ K, which are in reasonable agreement with experiment. This suggests that the superconductivity in

this system can be described by the conventional phonon mechanism. For more precise estimations of λ_{ph} and T_C , detailed information on the phonon spectra is prerequisite.

In conclusion, we have investigated electronic structures of the non-oxide antiperovskite superconductor MgCNi_3 . The π^* antibonding state of Ni-3d and C-2p is formed near E_F with the mainly Ni-3d character. Fermi surfaces are composed of two bands. The topology of hole Fermi surfaces coming from the 18th band is sensitively modified by the variance of the Fermi level position. The electron surface of the 19th band with an octahedron-cage shape tends to induce the Fermi surface nesting. By comparison of DOSs for MgXNi_3 ($X=\text{B,C,N}$), the doping effects are discussed. The estimation of λ_{ph} and T_c based on the rigid-ion approximation suggests that the superconductivity of MgCNi_3 is described well by the conventional phonon mechanism.

Acknowledgments – This work was supported by the KOSEF through the eSSC at POSTECH and in part by the BK21 Project. Helpful discussions with N.H. Hur are greatly appreciated.

¹ T. He, Q. Huang, A. P. Ramirez, Y. Wang, K. A. Regan, N. Rogado, M. A. Hayward, M. K. Haas, J. S. Slusky, K. Inumara, H. W. Zandbergen, N. P. Ong and R. J. Cava, *Nature (London)* **411**, 54 (2001).

² R. Nagarajan, Chandan Mazumdar, Zakir Hossain, S. K. Dhar, K. V. Gopalakrishnan, L. C. Gupta, C. Godart, B. D. Padalia, and R. Vijayaraghavan, *Phys. Rev. Lett.* **72**, 274 (1994).

³ R. J. Cava, H. Takagi, H. W. Zandbergen, J. J. Krajewski, W. F. Peck Jr, T. Siegrist, B. Batlogg, R. B. Can Dover, R. J. Felder, K. Mizuhashi, J. O. Lee, H. Eisaki and S. Uchida, *Nature (London)* **367**, 252 (1994).

⁴ W.E. Pickett and D.J. Singh, *Phys. Rev. Lett.* **72**, 3702 (1994); L. F. Mattheiss, *Phys. Rev. B* **49**, 13279 (1994); J. I. Lee, T. S. Zhao, I. G. Kim, B. I. Min, and S. J. Yoon, *Phys. Rev. B* **50**, 4030 (1994).

⁵ M. A. Hayward, M. K. Haas, A. P. Ramirez, T. He, K. A. Regan, N. Rogado, K. Inumara and R. J. Cava, *cond-mat/0104541*, (2001).

⁶ S.B. Dugdale and T. Jarlborg, *cond-mat/0105349*, (2001).

⁷ S. Y. Li, R. Fan, X. H. Chen, C. H. Wang, W. Q. Mo, K. Q. Ruan, Y. M. Xiong, X. G. Luo, H. T. Zhang, L. Li, Z. Sun and L. Z. Cao, *cond-mat/0104554*, (2001).

⁸ Z. Q. Mao, M. M. Rosario, K. Nelson, K. Wu, I. G. Deac, P. Schiffer and Y. Liu, T. He, K. A. Regan and R. J. Cava, *cond-mat/0105280*, (2001).

⁹ D.A. Papaconstantopoulos and W.E. Pickett, *Phys. Rev. B* **45**, 4008 (1992); P.R. Vansant, P.E. Van Camp, V.E. Van Doren, and J.L. Martins, *Phys. Rev. B* **57**, 7615 (1998); A.L. Ivanovskii, R.F. Sabiryanov, and A.N. Skazkin, *Fiz. Tverd. Tela*, **40**, 1667 (1998) (*Phys. Solid State* **40** 1516,

(1998)); W.S. Kim, E.O. Chi, J.C. Kim, H.S. Choi, and N.H. Hur (private communications).

¹⁰ S. H. Shim and B. I. Min (unpublished).

¹¹ Q. Huang, T. He, K. A. Regan, N. Rogado, M. Hayward, M. K. Haas, K. Inumara and R. J. Cava, *cond-mat/0105240* (2001).

¹² G. D. Gaspari and B. L. Gyorffy, *Phys. Rev. Lett.* **28**, 801 (1972).

¹³ W. L. McMillan, *Physical Review*, **167**, 331 (1967).

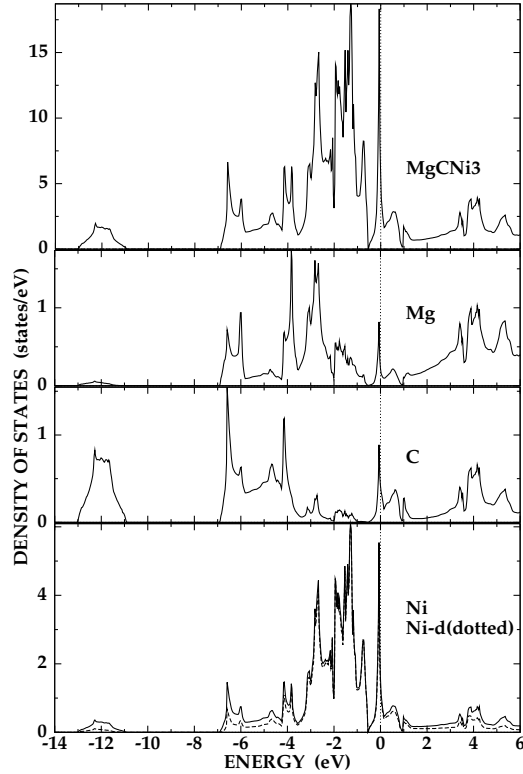


FIG. 1. Total and projected local DOS of MgCNi_3 .

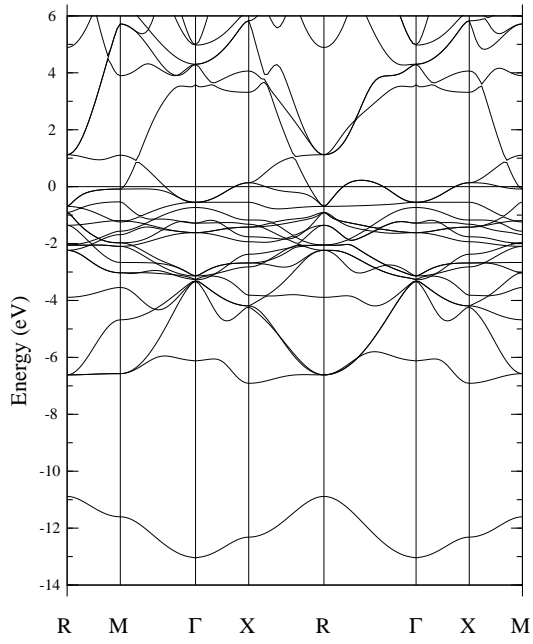


FIG. 2. Band structure of MgCNi_3 along the symmetry lines of the simple cubic Brillouin zone

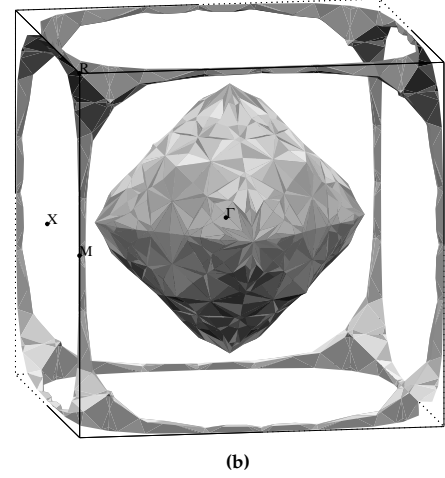
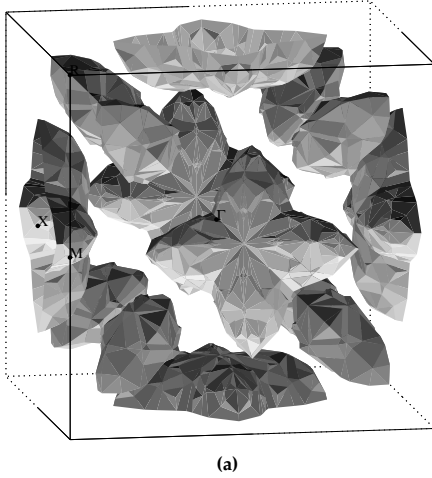


FIG. 3. Fermi surfaces of MgCNi_3 in the simple cubic Brillouin zone coming from the 18th band (a) and the 19th band (b)

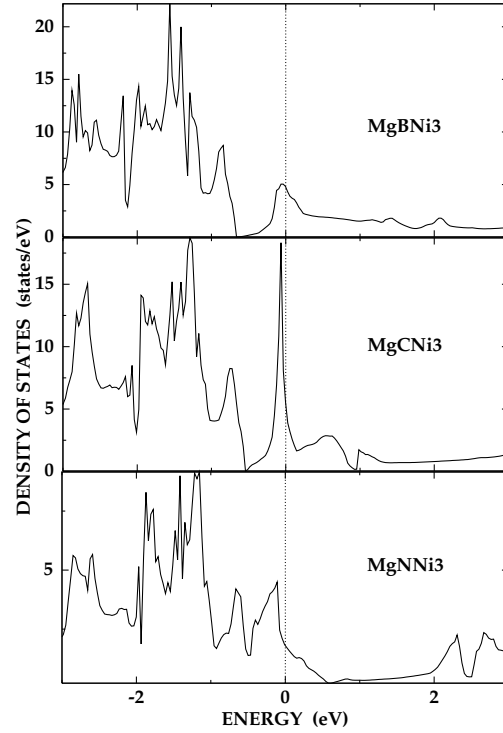


FIG. 4. Density of states of MgXNi_3 ($X = \text{B, C, N}$)

TABLE I. Total and partial DOSs at E_F (in states/eV) for MgXNi_3 ($X = \text{B, C, N}$).

| | N_{Mg} | N_X | N_{Ni} | N_{total} |
|------------------|-----------------|-------|-----------------|--------------------|
| MgBNi_3 | 0.38 | 0.18 | 1.41 | 4.79 |
| MgCNi_3 | 0.22 | 0.42 | 1.57 | 5.34 |

| | | | | |
|--------------------|------|------|------|------|
| MgNNi ₃ | 0.11 | 0.34 | 1.06 | 3.63 |
|--------------------|------|------|------|------|

TABLE II. Comparison of η (in eV/Å²) and λ_{ph} for $\Theta_D=300\text{K}$ and 400K .

| | η_{Mg} | η_{X} | η_{Ni} | λ_{ph} (300K) | λ_{ph} (400K) |
|--------------------|--------------------|-------------------|--------------------|-----------------------|-----------------------|
| MgBNi ₃ | 0.00 | 0.22 | 0.67 | 0.67 | 0.38 |
| MgCNi ₃ | 0.00 | 0.48 | 1.36 | 1.36 | 0.77 |
| MgNNi ₃ | 0.00 | 0.58 | 0.87 | 1.07 | 0.60 |